Electronic Supplementary Material (ESI) for Materials Chemistry Frontiers.

Scalable synthesis of pyrazine-linked conjugated microporous polymers for high-performance proton conduction

Gang Yuan, Hao Luo, Zhenhua Li, Yuze Chen, Bangdi Ge, Xiaowei Song* and Zhiqiang Liang*

State Key Laboratory of Inorganic Synthesis and Preparative Chemistry, College of Chemistry, Jilin University, Changchun 130012, P. R. China

*Corresponding Authors.

E-mail addresses: xiaoweisong@jlu.edu.cn (X. W. Song), liangzq@jlu.edu.cn (Z. Q. Liang).

Materials and characterizations

All chemicals were obtained from commercial suppliers and used without further purification. Fourier transform infrared (FT-IR) spectra were recorded in the range of 400−4000 cm^{-1} on a Nicolet 6700 FT-IR spectrometer with KBr pellets. X-ray photoelectron spectroscopy (XPS) were performed using an ESCALAB 250 spectrometer with a monochromatic X-ray source (Al Kα hυ = 1486.6 eV). The X-ray diffraction (XRD) patterns were recorded using a Rigaku D/Max 2550 X-ray diffractometer (Cu Kα radiation, λ=1.5418 Å). The content of metal in products were determined with inductively coupled plasma (ICP) analyses carried out on a Perkin-Elmer Optima 3300 DV ICP instrument. Elemental analyses (C, H, and N) were performed with a Vario MICRO (Elementar, Germany). Surface morphologies were characterized using a JSM-7800 F field emission scanning electron microscope (SEM) at an accelerating voltage of 3 kV. Transmission electron microscopy (TEM) were conducted on a FEI Tecnai G2S-Twin with a field emission gun operating at 200 kV. Thermal gravimetric analyses (TGA) were carried out on a TGA Q500 thermogravimetric analyzer in air atmosphere at a heating rate of 10 °C min^{-1}. Micromeritics ASAP 2020 instrument was used to evaluate the adsorption properties of N_2 with the samples degassed at 120 °C for 10 h before testing under high vacuum. Solution-state ^{1}H spectra and solution-state ^{13}C spectra were recorded on a Varian Mercury spectrometer operating at frequency of 300 and 75 MHz, respectively.

Experimental section

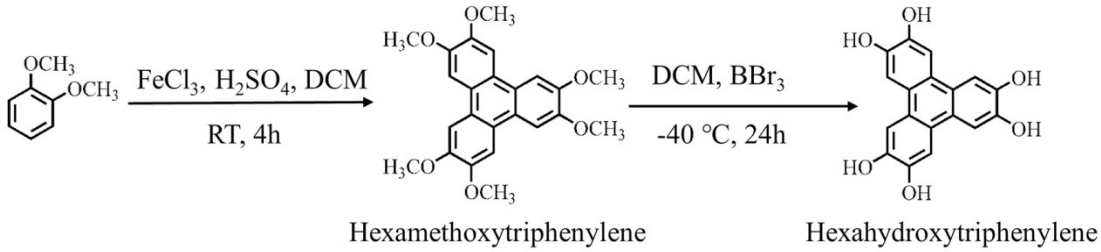

Fig. S1 Synthesis of hexahydroxytriphenylene.

Synthesis of Hexamethoxytriphenylene

Anhydrous $FeCl_3$ (17.6 g) was added into a mixed solvent of CH_2Cl_2 (75 mL) and concentrated H_2SO_4 (0.15 mL). After adding the CH_2Cl_2 (50 mL) solution containing phthalic ether (13.6 g, 99 mmol) dropwise within 10 min, the resulting mixture was further stirred for 4 h at room temperature. Then MeOH (100 mL) was added slowly and the solution was stirred for additional 30 min. By filtering off the precipitate, washing with MeOH (200 mL) and drying under vacuum, the slightly beige products were obtained (9.7 g, 72.3%). ^{1}H NMR (300 MHz, CDCl3) = 7.81 (*s*, 1H), 4.13 (*s*, 3H) ppm).

Synthesis of hexahydroxytriphenylene.

Hexamethoxytriphenylene (2.04, 5.0 mmol) was dissolved in CH_2Cl_2 (50 mL) and cooled to 0 ℃ using an ice bath and stirred. A precooled (0 ℃) CH_2Cl_2 solution containing BBr_3 (1 M in CH_2Cl_2, 60 mL) was added and mixture was stirred for another 24 h at room temperature. Next, deionized water (200 mL) was slowly added into the reaction and the mixture was stirred for an additional 1 h. The mixture was extracted with EA and then washed with brine solution. After drying by anhydrous $MgSO_4$, the solution was removed under reduced pressure and grey products were obtained (1.26 g,

77.8%). ^{1}H NMR (300 MHz, DMSO-*d*6) = 9.27 (*s*, 6H), 7.64 (*s*, 6H) ppm.

Synthesis of HD-CMP2

The synthesis of **HD-CMP2** was performed by the solvothermal condensation reaction of hexahydroxy triphenylene (HHTP, 0.97 g, 3.0 mmol), 3,3'-diaminobenzidine (DABZ) (0.963 g, 4.5 mmol) and DDQ (4.08 g, 18 mmol) in a mixture solvent of 1,4-dioxane, ethylene glycol and N-methylpyrrolidone (NMP) (52 mL, 20:5:1). Initially, the reaction mixture was stirred for 2 hours before adding 1 mL acetic acid under air atmosphere. The resulting gel was stirred for an additional 2 hours before it was transferred to a 100 mL Teflon lined stainless steel autoclave and heated to 150 °C for 3 days under static conditions. The resultant black precipitate was isolated by filtration and washed with 0.1 M hydrochloric acid, ethanol and tetrahydrofuran (THF), respectively. The sample was transferred to a Soxhlet extractor and washed with dichloromethane for 24 hours and then dried at 80 °C under vacuum for 24 h to give black powders.

Preparation of Im@HD-CMP

Im@HD-CMP were prepared by a vapor diffusion method. A glass vial containing **HD-CMP** was put into an autoclave with excess imidazole placed outside the glass vial. The autoclave was sealed and transferred to an oven and heated to 150 °C. The imidazole was vaporized into the pores of **HD-CMP**.

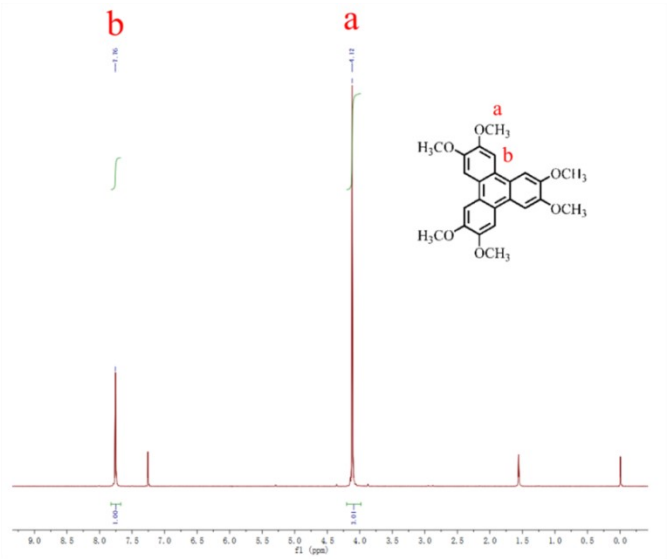

Fig. S2 [1]H NMR (300 MHz, CDCl3, 298 K) spectrum of hexamethoxytriphenylene.

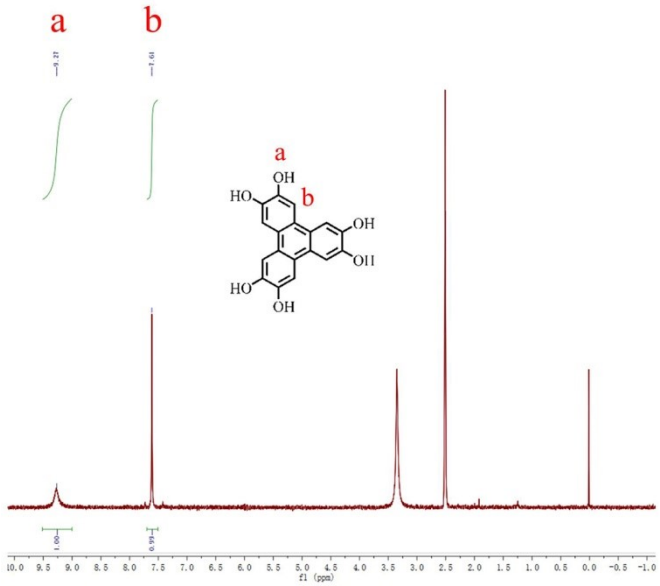

Fig. S3 [1]H NMR (300 MHz, DMSO-d_6) spectrum of hexahydroxytriphenylene.

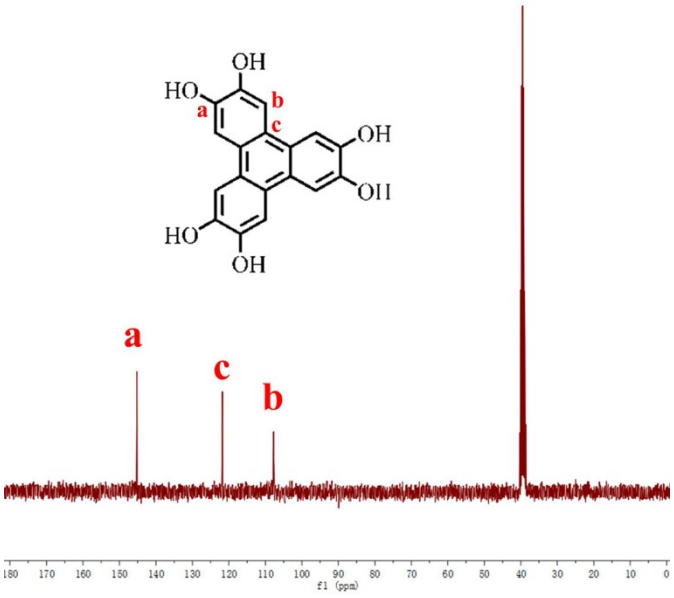

Fig. S4 ^{13}C NMR (75 MHz, DMSO-d_6) spectrum of hexahydroxytriphenylene.

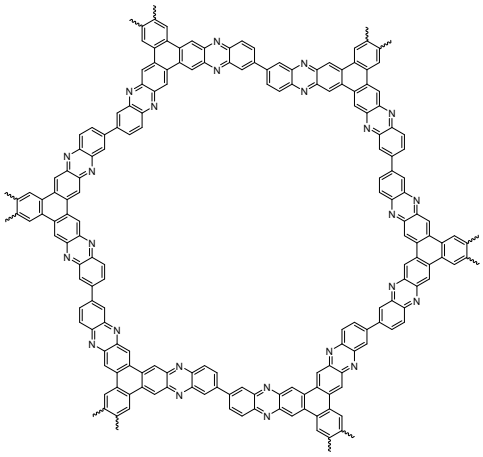

Fig.S5 The structure of **HD-CMP2**

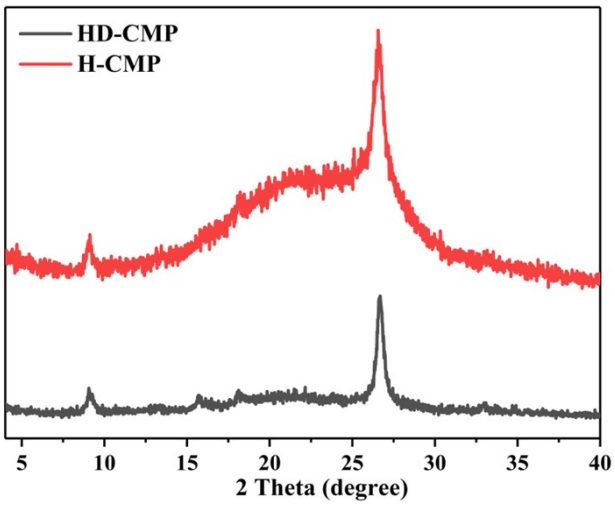

Fig. S6 PXRD patterns of the **HD-CMP** and **H-CMP**.

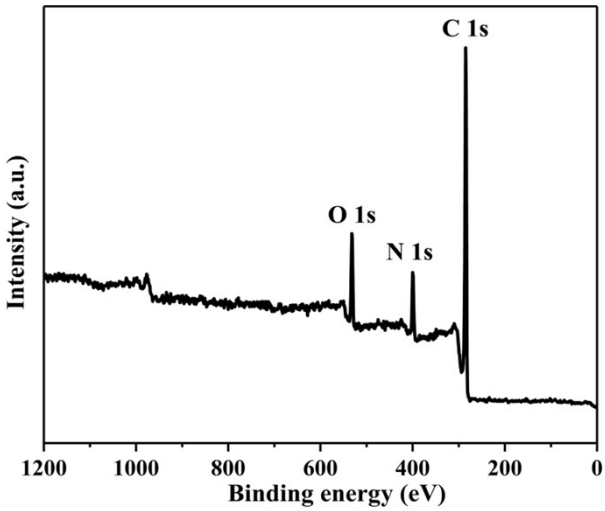

Fig. S7 XPS survey spectrum of **HD-CMP**.

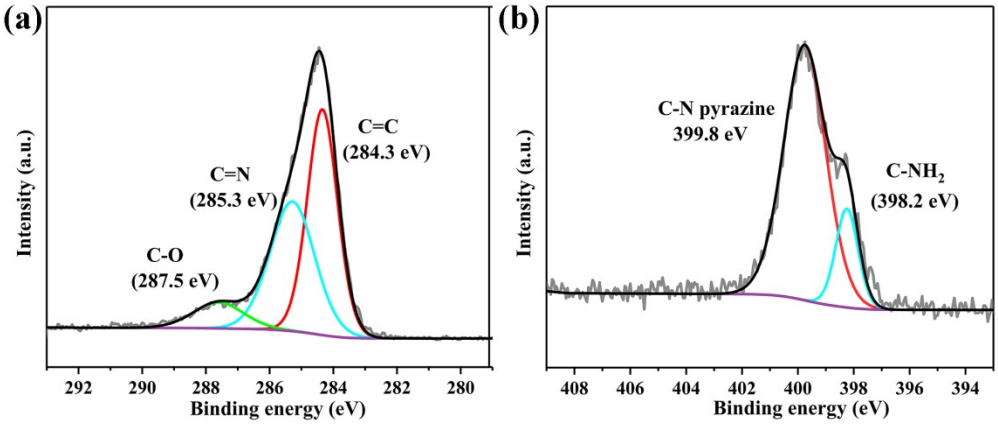

Fig. S8 (a) C1s spectrum of **HD-CMP**. (b) N1s spectrum of **HD-CMP**.

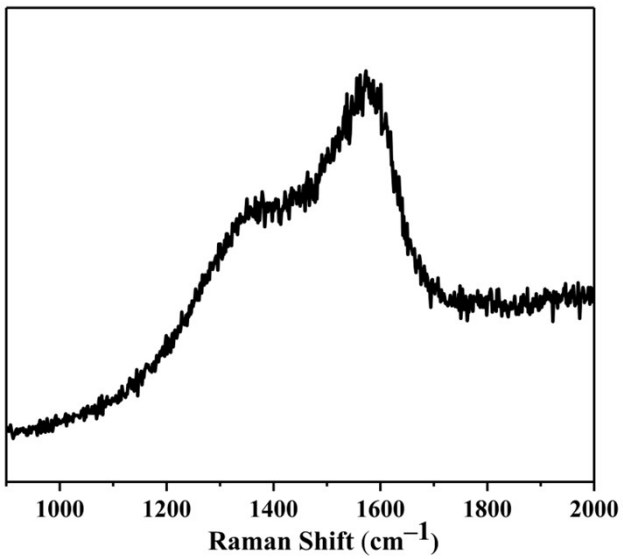

Fig. S9 Raman spectrum of **HD-CMP**.

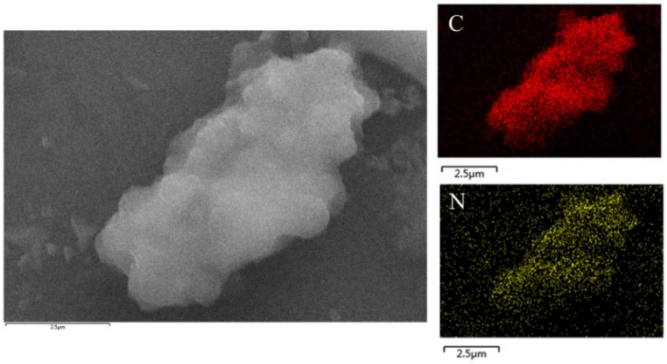

Fig. S10 SEM & EDS mapping images of **HD-CMP**.

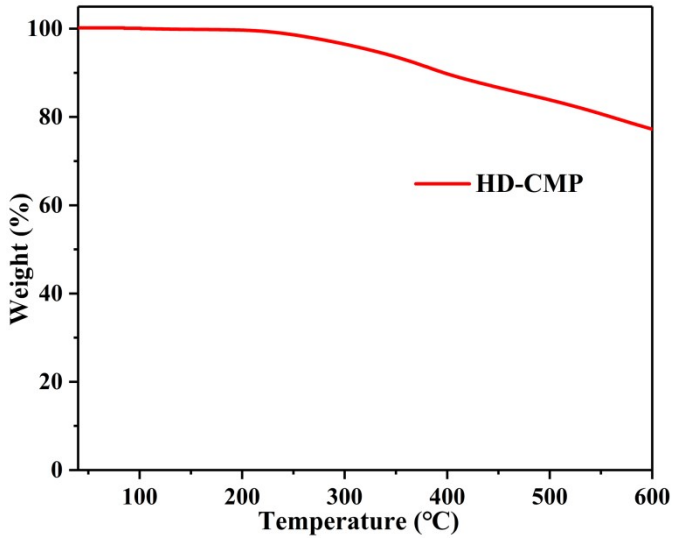

Fig. S11 TGA curve of **HD-CMP** under N_2 atmosphere.

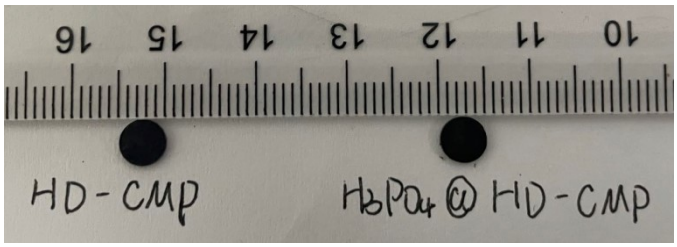

Fig. S12 Digital photographs of **HD-CMP** and **H_3PO_4@HD-CMP** pellets.

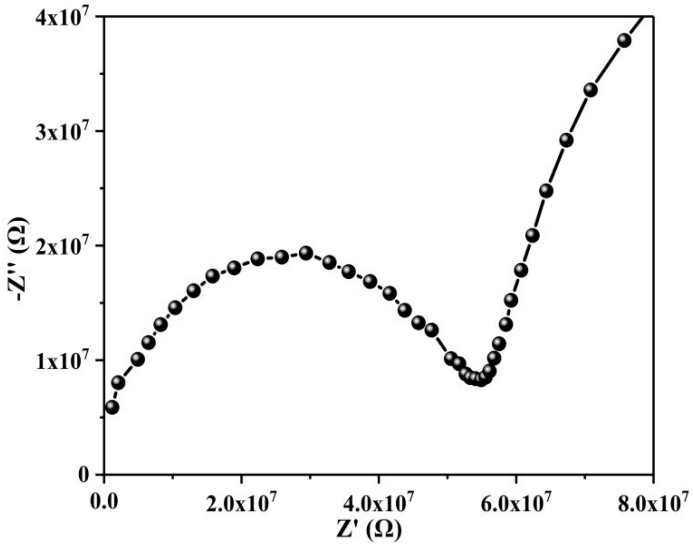

Fig. S13 Nyquist plot of **HD-CMP** at 298 K under anhydrous condition.

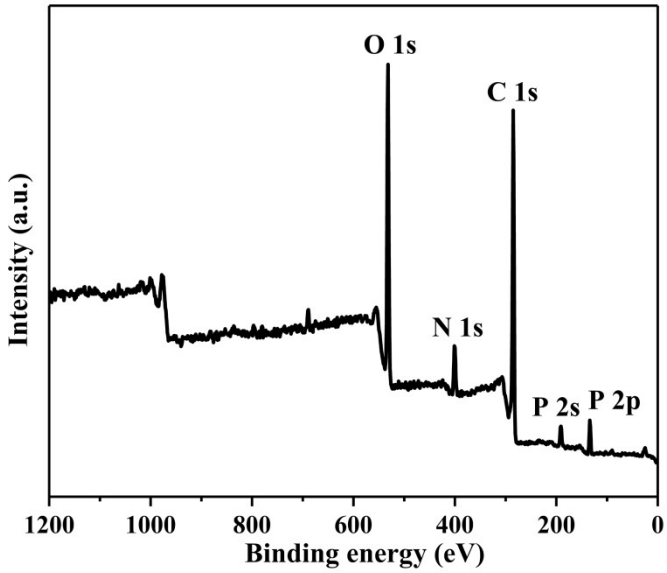

Fig. S14 XPS survey spectrum of **H3PO4@HD-CMP**.

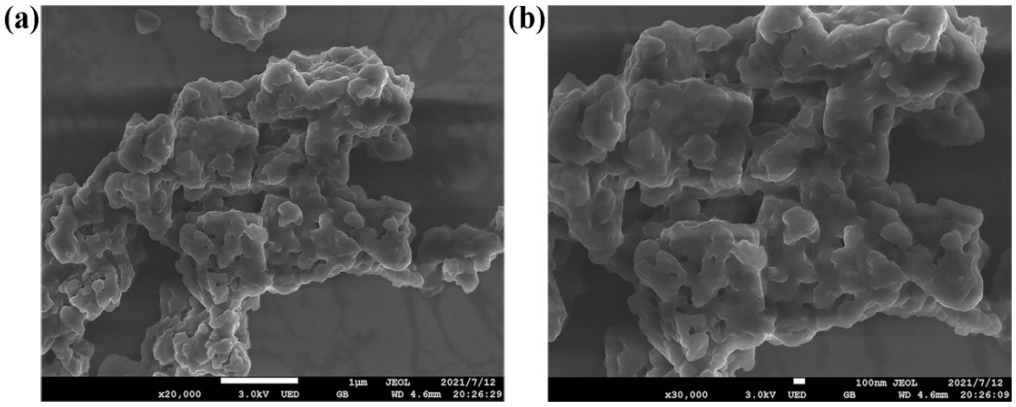

Fig. S15 SEM images of **H_3PO_4@HD-CMP**.

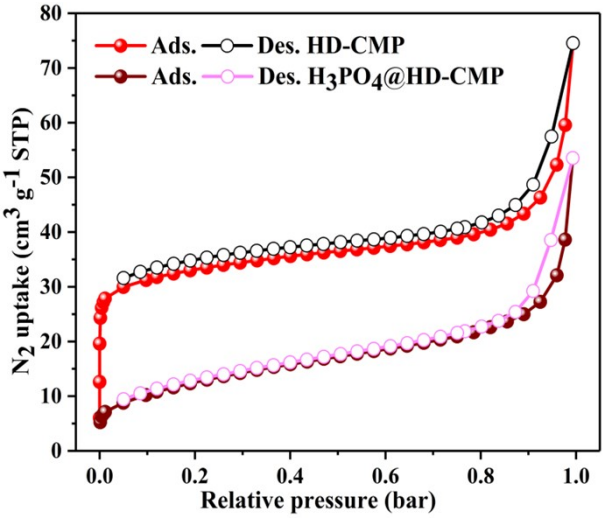

Fig. S16 N_2 adsorption and desorption isotherms of **HD-CMP** and **H_3PO_4@HD-CMP** at 77 K.

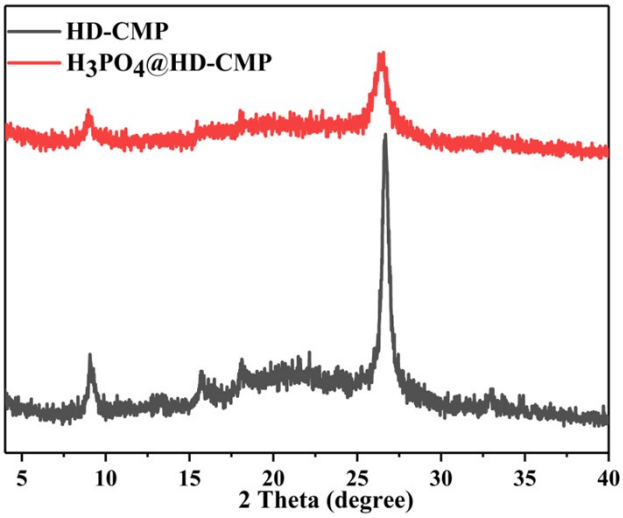

Fig. S17 PXRD of **H_3PO_4@HD-CMP** compared with **HD-CMP**.

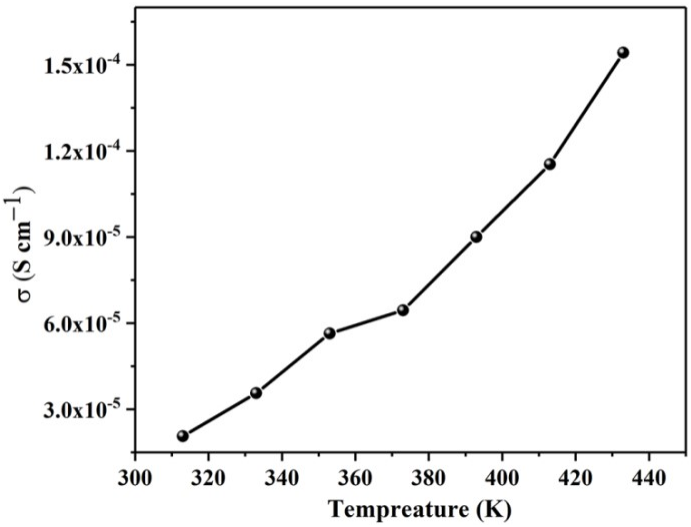

Fig. S18 Proton conductivities of **H_3PO_4@HD-CMP** measured at different temperature under anhydrous condition.

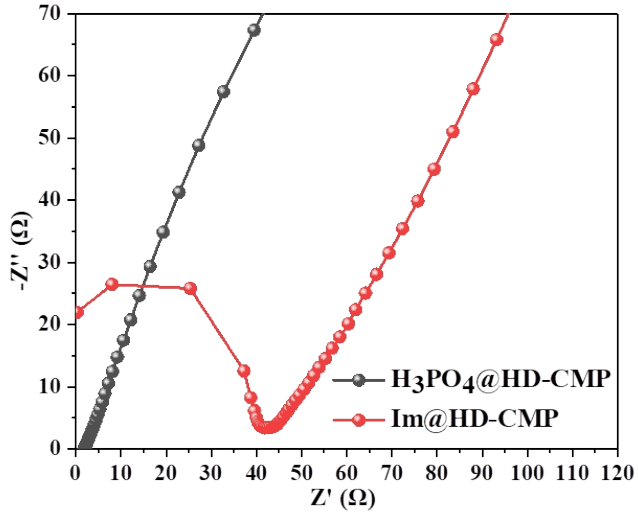

Fig. S19 Nyquist plots of **H_3PO_4@HD-CMP** and **Im@HD-CMP** measured under 100% RH at 353 K.

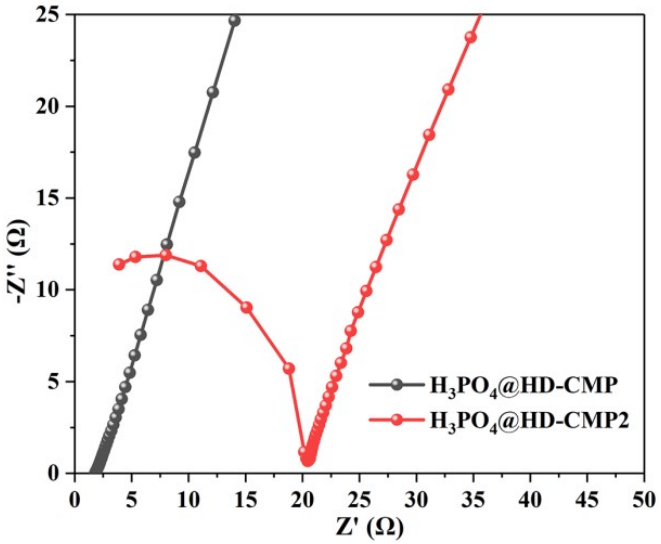

Fig. S20 Nyquist plots of **H_3PO_4@HD-CMP** and **H_3PO_4@HD-CMP2** measured under 100% RH at 353 K.

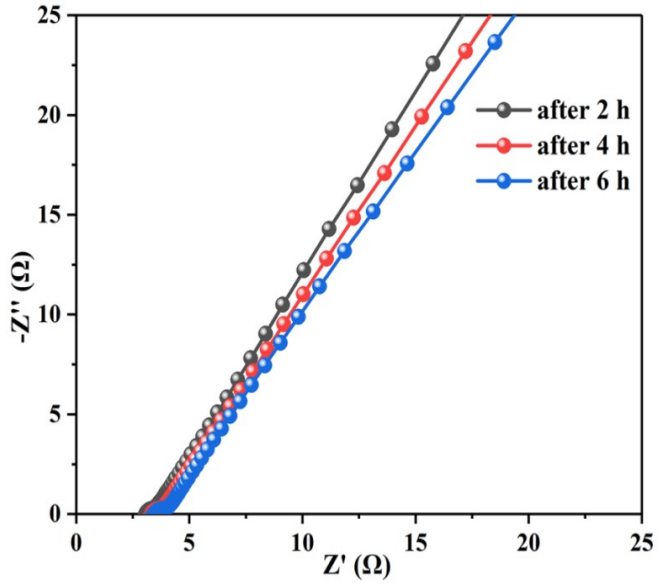

Fig. S21. Nyquist plots of **H_3PO_4@HD-CMP** measured at 333 K under 100% RH for 6 consecutive hours in a constant temperature and humidity.

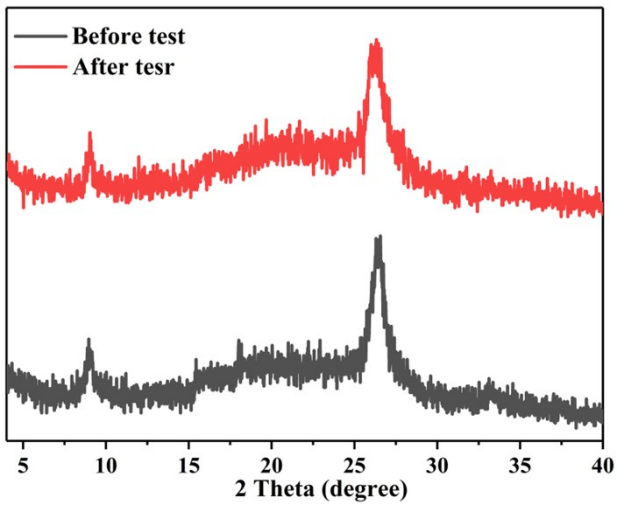

Fig. S22 PXRD patterns of **H_3PO_4@HD-CMP** before and after EIS test.

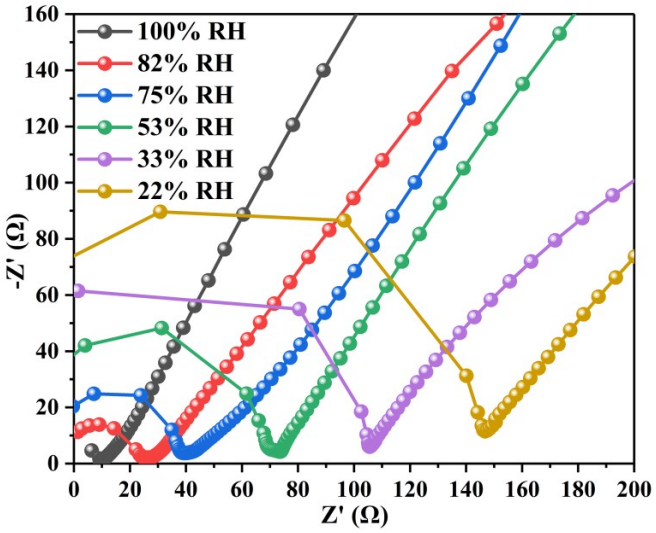

Fig. S23 Nyquist plots of **H_3PO_4@HD-CMP** measured at 298 K under different relative humidity.

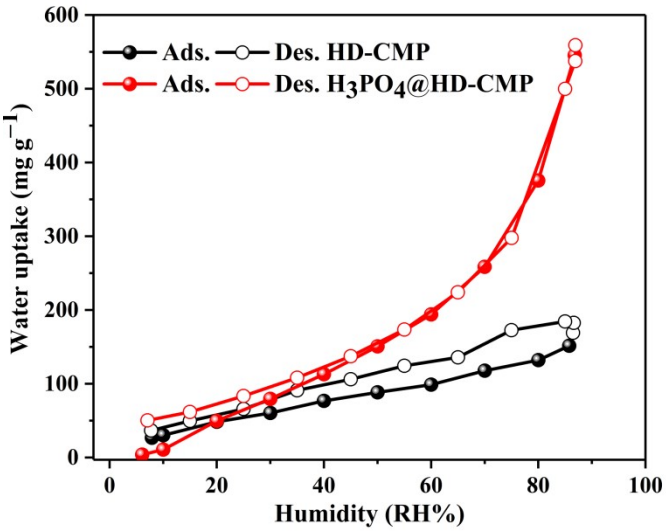

Fig. S24 Water vapor adsorption isotherms of **HD-CMP** and **H_3PO_4@HD-CMP** at 298 K.

Table S1 CHN elemental analysis and ICP results.

Sample	CHN Elemental Analysis (%)			phosphoric acid content (wt%)
	C	H	N	
HD-CMP	45.26	4.714	13.28	0
H_3PO_4@HD-CMP	42.63	4.069	8.43	4.2
H_3PO_4@HD-CMP (after six hours)	42.37	3.945	8.30	4.1

Table S2 List of the proton conductive materials based on porous organic materials.

System	T (K)	RH (%)	σ (S cm^{-1})	Ea (eV)	Reference
H_3PO_4@HD-CMP	353	100	1.05×10^{-1}	0.20	This work
Nafion	353	98	$\sim1\times10^{-1}$	0.22	S1
H_3PO_4@NKCOF-10	353	90	9.04×10^{-2}	0.06	S2
PTSA@TpAzo	353	95	7.8×10^{-2}	0.11	S3
aza-COF-2_H	323	97	4.8×10^{-3}	0.29	S4
H_3PO_4@NKCOF-1	353	98	1.13×10^{-1}	0.14	S5
EB-COF:PW_{12}	298	97	3.32×10^{-3}	0.24	S6
BIP	368	95	3.2×10^{-2}	0.31	S7
PA@Tp-Azo	333	98	9.9×10^{-4}	0.11	S8
P2PV	298	75	1.7×10^{-2}	/	S9
SCOF	353	Pure water	5.4×10^{-1}	0.19	S10
NUS-10	298	98	3.96×10^{-2}	/	S11
S-COF-2	298	95	1.5×10^{-2}	0.17	S12
1S3MP	353	90	2.13×10^{-2}	0.039	S13
H_3PO_4@TPB-DMeTP-COF	433	Anhydrous	1.9×10^{-1}	0.34	S14
COF-F6-H (62 wt% H_3PO_4 loadings	413	Anhydrous	4.2×10^{-2}	/	S15
PA@EB-COF	453	Anhydrous	2.77×10^{-2}	0.35	S16
H@TPT-COF	433	Anhydrous	1.27×10^{-2}	0.17	S17
TFPPY-BT-COF-H_2PO_3	333	98	1.12×10^{-3}	0.20	S18
PAPOP-DD-0.5	348	98	7.09×10^{-2}	0.28	S19
MOF-808-IMDC	353	98	1.11×10^{-2}	0.25	S20
MFM-300(Cr)-$SO_4(H_3O)_2$	293	99	1.26×10^{-2}	0.04	S21
S-POP-TPM	353	98	1.0×10^{-1}	0.23	S22
LiCl@PRH	363	90	5.4×10^{-1}	0.34	S23
HOF-GS-11	303	60	2.6×10^{-4}	0.48	S24
NiOF-1	328	95	3.14×10^{-2}	/	S25

Table S3 The electronic conductivity **HD-CMP** and **H_3PO_4@HD-CMP** of under at room temperature under 53% RH

Sample	Resistance (MΩ)					Average (MΩ)	ρ (Ω× cm)	σ (S cm^{-1})
HD-CMP	28.6	27.4	28.5	29.6	27.2	28.26	1.413×10^6	7.07×10^{-7}
H_3PO_4@HD-CMP	43.7	42.8	42.2	45.2	43.3	43.44	2.172×10^6	4.60×10^{-7}

The electronic conductivity was calculated by the formula:
$\rho = R \times F(D/S) \times F(W/S) \times Fsp \times W$ (Ω × cm)
$\sigma = 1 / \rho$
F(D/S) = 1; F(W/S) = 1; Fsp = 1
W = 0.05 cm

Table S4 The proton conductivity **H_3PO_4@HD-CMP** measured at 298 K under different relative humidity.

RH (wt%)	22	33	53	75	82	100
R (Ω)	146	105	68	37	24	10
σ (S cm^{-1})	2.09×10^{-3}	2.91×10^{-3}	4.50×10^{-3}	8.26×10^{-3}	1.27×10^{-2}	3.05×10^{-2}

The proton conductivity was calculated by the formula:
$\sigma = L / (RA)$
L = 0.06 cm
A = 0.19625 cm^2
R is the resistance of the pellet (Ω) corresponding to the real Z' Nyquist plot

Table S5 The proton conductivity **H_3PO_4@HD-CMP** measured at 100% RH under different temperature.

Temperature (K)	303	313	323	333	343	353
R (Ω)	7.7	6.8	5.3	4.4	3.5	2.9
σ (S cm^{-1})	3.97×10^{-2}	4.49×10^{-2}	5.76×10^{-2}	6.94×10^{-2}	8.73×10^{-2}	1.05×10^{-1}

The proton conductivity was calculated by the formula:
$\sigma = L / (RA)$
L = 0.06 cm
A = 0.19625 cm^2
R is the resistance of the pellet (Ω) corresponding to the real Z' Nyquist plot

Table S6 The purity of reagents used in this work.

Reagent	Purity (%)
1,4-dioxane	99.5
mesitylene	97
NMP	99
ethylene glycol	99
1,2,4,5-benzenetetramine tetrahydrochloride	95
1,2-Dimethoxybenzene	98
H_3PO_4	85

Reference

S1 X. Wu, X. Wang. G. He and J. Benziger, Differences in water sorption and proton conductivity between Nafion and SPEEK, *J. Polym. Sci., Part B: Polym. Phys.*, 2011, **49**, 1437-1445.

S2 Z. Wang, Y. Yang, Z. Zhao, P. Zhang, Y. Zhang, J. Liu, S. Ma, P. Cheng, Y. Chen and Z. Zhang, Green synthesis of olefin-linked covalent organic frameworks for hydrogen fuel cell applications, *Nat. Commun.*, 2021, **12**, 1982.

S3 H. S. Sasmal, H. B. Aiyappa, S. N. Bhange, S. Karak, A. Halder, S. Kurungot, and R. Banerjee, Superprotonic conductivity in flexible porous covalent organic framework membranes. *Angew. Chem. Int. Ed.*, 2018, **57**, 10894-10898.

S4 Z. Meng, A. Aykanat and K. A. Mirica, Proton conduction in 2D aza-fused covalent organic frameworks, *Chem. Mater.*, 2019, **31**, 819-825.

S5 Y. Yang, X. He, P. Zhang, Y. H. Andaloussi, H. Zhang, Z. Jiang, Y. Chen, S. Ma, P. Cheng, and Z. Zhang, Combined intrinsic and extrinsic proton conduction in robust covalent organic frameworks for hydrogen fuel cell applications. *Angew. Chem. Int. Ed.*, 2020, **59**, 3678-3684.

S6 H. Ma, B. Liu, B. Li, L. Zhang, Y.-G. Li, H.-Q. Tan, H.-Y. Zang and G. Zhu, Cationic covalent organic frameworks: A simple platform of anionic exchange for porosity tuning and proton conduction, *J. Am. Chem. Soc.*, 2016, **138**, 5897-5903.

S7 C. R. Kayaramkodath, I. Rajith, D. V. Sairam, P. Joseph, C. W. Vivek, K. V. R. Goudappagouda, K. Sreekumar and S. B. Sukumaran, Imidazole-linked crystalline two-dimensional polymer with ultrahigh proton-conductivity. *J. Am. Chem. Soc.*, 2019, **141**, 14950-14954.

S8 S. Chandra, T. Kundu, S. Kandambeth, R. BabaRao, Y. Marathe, S. M. Kunjir and R. Banerjee, Phosphoric acid loaded azo (−N═N−) based covalent organic framework for proton conduction, *J. Am. Chem. Soc.*, 2014, **136**, 6570-6573.

S9 T. Jadhav, Y. Fang, C.-H. Liu, A. Dadvand, E. Hamzehpoor, W. Patterson, A. Jonderian, R. S. Stein and D. F. Perepichka, Transformation between 2D and 3D covalent organic frameworks via reversible [2 + 2] cycloaddition. *J. Am. Chem. Soc.*, 2020, **142**, 8862-8870.

S10 L. Liu, L. Yin, D. Cheng, S. Zhao, H.-Y. Zang, N. Zhang and G. Zhu, Surface-mediated construction of an ultrathin free-standing covalent organic framework membrane for efficient proton conduction. *Angew. Chem. Int. Ed.*, 2021, **60**, 14875-14880.

S11 Y. Peng, G. Xu, Z. Hu, Y. Cheng, C. Chi, D. Yuan, H. Cheng and D. Zhao, Mechanoassisted synthesis of sulfonated covalent organic frameworks with high intrinsic proton conductivity, *ACS Appl. Mater. Interfaces*, 2016, **8**, 18505-18512.

S12 L. Zhai, Y. Yao, B. Ma, M. M. Hasan, Y. Han, L. Mi, Y. Nagao and Z. Li, Accumulation of sulfonic acid groups anchored in covalent organic frameworks as an intrinsic proton-conducting electrolyte, *Macromol. Rapid Commun.*, 2021, **43**, 2100590.

S13 D. W. Kang, K. A. Lee, M. Kang, J. M. Kim, M. Moon, J. H. Choe, H. Kim, D. W. Kim, J. Y. Kim and C. S. Hong, Cost-effective porous-organic-polymer-based electrolyte membranes with superprotonic conductivity and low activation energy. *J. Mater. Chem. A*, 2020, **8**, 1147-1153.

S14 S. Tao, L. Zhai, A. D. Dinga Wonanke, M. A. Addicoat, Q. Jiang and D. Jiang Confining H_3PO_4 network in covalent organic frameworks enables proton super flow. *Nat. Commun.*, 2020, **11**, 1981.

S15 X. Wu, Y.-L. Hong, B. Xu, Y. Nishiyama, W. Jiang, J. Zhu, G. Zhang, S.

Kitagawa, and S. Horike, Perfluoroalkyl-functionalized covalent organic frameworks with superhydrophobicity for anhydrous proton conduction. *J. Am. Chem. Soc.*, 2020, **142**, 14357-14364.

S16 S. Chen, Y. Wu, Y. Zhang, W. Zhang, Y. Fu, W. Huang, T. Yan and H. Ma, Tuning proton dissociation energy in proton carrier doped 2D covalent organic frameworks for anhydrous proton conduction at elevated temperature, *J. Mater. Chem. A*, 2020, **8**, 13702-13709.

S17 G. Jiang, W. Zou, Z. Ou, L. Zhang, W. Zhang, X. Wang, H. Song, Z. Cui, Z. Liang and L. Du, Tuning the interlayer interactions of 2D covalent organic frameworks enables an ultrastable platform for anhydrous proton transport. *Angew. Chem. In. Ed.*, 2022, **61**, e202208086.

S18 Z. Lu, C. Yang, L. He, J. Hong, C. Huang, T. Wu, X. Wang, Z. Wu, X. Liu, Z. Miao, B. Zeng, Y. Xu, C. Yuan and L. Dai, Asymmetric hydrophosphonylation of imines to construct highly stable covalent organic frameworks with efficient intrinsic proton conductivity, *J. Am. Chem. Soc.*, 2022, **144**, 9624-9633.

S19 T. Zhu, B. Shi, H. Wu, X. You, X. Wang, C. Fan, Q. Peng and Z. Jiang, Highly proton conductive phosphoric acid porous organic polymers via knitting method, *Ind. Eng. Chem. Res.*, 2021, **60**, 6337-6343.

S20 X.-M. Li, Y. Wang, Y. Mu, J. Gao and L. Zeng, Oriented construction of efficient intrinsic proton transport pathways in MOF-808, *J. Mater. Chem. A*, 2022, **10**, 18592-18597.

S21 J. Chen, Q. Mei, Y. Chen, C. Marsh, B. An, X. Han, I. P. Silverwood, M. Li, Y. Cheng, M. He, X. Chen, W. Li, M. Kippax-Jones, D. Crawshaw, M. D. Frogley, S. J. Day, V. García-Sakai, P. Manuel A. J. Ramirez-Cuesta, S. Yang and M. Schröder, Highly efficient proton conduction in the metal–organic framework material MFM-300(Cr)·$SO_4(H_3O)_2$, *J. Am. Chem. Soc.*, 2022, **144**, 11969-11974.

S22 Z. Li, Y. Yao, D. Wang, M. M. Hasan, A. Suwansoontorn, H. Li, G. Du, Z. Liu and Y. Nagao, Simple and universal synthesis of sulfonated porous organic polymers with high proton conductivity, *Mater. Chem. Front.*, 2020, **4**, 2339-2345.

S23 D. Taylor, X. Hu, C.-M. Wu, J. M. Tobin, Z. Oriou, J. He, Z. Xu and F. Vilela,

Superprotonic conduction of intrinsically zwitterionic microporous polymers based on easy-to-make squaraine, croconaine and rhodizaine dyes, *Nanoscale Adv.*, 2022, **4**, 2922-2928.

S24 A. Karmakar, R. Illathvalappil, B. Anothumakkool, A. Sen, P. Samanta, A. V. Desai, S. Kurungot and S. K. Ghosh, Hydrogen-bonded organic frameworks (HOFs): A new class of porous crystalline proton-conducting materials, *Angew. Chem. Int, Ed.*, 2016, **55**, 10667-10671.

S25 H. Gao, Y.-B. He, J.-J. Hou and X.-M. Zhang, In situ aliovalent nickle substitution and acidic modification of nanowalls promoted proton conductivity in InOF with 1D helical channel, *ACS Appl. Mater. Interfaces*, 2021, **13**, 38289-38295.